https://doi.org/10.1016/j.cej.2021.131698

Fiber-Shaped Stretchable Triboelectric Nanogenerator with a Novel Synergistic Structure of Opposite Poisson's Ratios

Xiaoyang Guan, Bingang Xu*, Junxian Huang, Titao Jing, Yuanyuan Gao

† Nanotechnology Center, Institute of Textiles and Clothing, The Hong Kong Polytechnic University, Hung Hom, Kowloon, Hong Kong, P. R. China

* Corresponding author. E-mail: tcxubg@polyu.edu.hk; Tel: +852-2766 4544

ABSTRACT: The rapid advancement of flexible and stretchable electronics has attracted intensive attention in recent decades. However, challenges still remain in developing wearable and sustainable power sources with comparable portability and stretchability. Here, a novel type of stretchable fiber-shaped triboelectric nanogenerator (AXF-TENG) was fabricated by inserting a negative Poisson-ratio auxetic fiber into a positive Poisson-ratio hollow circular sleeve, forming a synergistic structured TENG composed of opposite Poisson's ratios. Owing to the advanced structural designs, the inner auxetic fiber would expand in all directions to more effectively contact with the shrunk outer steel wire sleeve under stretching. The peak-to-peak voltage and transfer charge of composite based AXF-TENG could reach up to 42 V and 12.5 nC, respectively. The fabricated AXF-TENG can be used as a self- powered multifunctional sensor to detect human motions and be woven into an energy-harvesting fabric to scavenge biomechanical energy. With open-circuit voltage of 46 V and maximum instantaneous power density of 52.36 mW/m^2, the AXF-TENG fabric was capable of lighting up 20 light emitting diodes (LEDs), charging commercial capacitors, powering an electronic watch and a calculator. All of these merits of the proposed AXF-TENGs suggest their promising potentials for versatile applications in biomechanical energy harvesting and self-powered sensing.

KEYWORDS: Triboelectric nanogenerator; Opposite Poisson's ratios; Stretchable electronics; Self-powered sensor; Energy harvesting

1. Introduction

In recent years, with the rapid advancements in flexible and wearable electronic devices such as intelligent glasses, smart watches, artificial electronic skins[1], healthcare monitoring sensors[2] and so forth, the urgent demands for flexible, stretchable, and sustainable power sources have been attracting intensive interest[3]. Nevertheless, traditional power sources like conventional batteries and capacitors are becoming more unfavorable to meet the energy requirements of these wearable electronics, due to their rigid framework, heavy weight, large volume, limited capacity and lifetime, and lack of flexibility[4–6]. To address this issue, energy harvesting technologies, which can scavenge renewable and sustainable energy from ambient environment or human motions based on piezoelectric[7], triboelectric[8,9], photovoltaic[10], or thermoelectric effects[11], have been developed as fundamental and effective approaches to solve the sustainable power supply challenge[12]. Among the various energy harvesting technologies, the emerging triboelectric nanogenerator (TENG), which can effectively convert various types of mechanical energy into electricity based on coupling effects of triboelectrification and electrostatic induction, is one of the most promising alternatives for powering wearable devices owing to its advantages of high output performance, low cost, simple fabrication, versatile structural designs, wide choices of materials and environment-friendly features[13,14]. Moreover, distinguished from photovoltaic and thermoelectric energy harvesting strategies, triboelectric energy harvesting is nearly independent of weather and environment[15]. Hence, extensive efforts have been made to fabricate TENGs for the promising

applications in self-powered active sensors[16–18], sustainable energy sources[19] and wearable multifunctional intelligent systems[20,21].

To date, most TENGs appear in planar or thin-film structures with limited flexibility, stretchability and comfortability, which are difficult for integration with clothing and adaption to large deformation of human motion in diverse directions[22–24]. To this end, stretchable one-dimensional TENGs that have conspicuous advantages of compactness, lightweight, good flexibility, high deformability and wearing comfort are highly desired[25–28]. In particular, they are promising to be easily integrated with other electronics and woven into fabrics[29–35]. Recently, several efforts have been made to prepare stretchable fiber-shaped TENGs with different configuration designs such as two-fiber-twisted structure[30,36], coaxial structure[37–39], helical-structure[40], and so on. Among them, stretchable nanogenerators with coaxial core-shell fiber structures were demonstrated to be more favorable candidates owing to their exceptional structure stability under various deformations and better output performance[41]. The key working principle of these coaxial core-shell fiber-shaped TENGs is based on the reversable distance change induced by the reversable distance change between the core fiber and the shell during tensile deformation[39,42]. However, in previous studies, although various approaches have been taken to optimize the materials selection and structure design, almost all core fibers and shell used were still conventional materials without synergistic and opposite Poisson's ratios, which inherently limited the energy harvesting performance and sensitivity of mechanical

deformation due to the ineffective contact between triboelectric materials induced by the small Poisson's ratio difference between the core fiber and the shell[43].

Herein, a novel type of stretchable fiber-shaped triboelectric nanogenerator with a unique core-shell coaxial architecture for biomechanical energy harvesting and human motion sensing was designed and fabricated, in which a brand-new negative Poisson-ratio auxetic core fiber was axially inserted into a commercial hollow circular sleeve with positive Poisson's ratio, forming a synergistic structured TENG composed of opposite Poisson's ratios. The developed auxetic core fiber, which would expand in all directions under stretching, was rationally designed by selecting a helical-structure stainless steel yarn as the stretchable electrode and employing polydimethylsiloxane (PDMS) to cover the spiral stainless-steel yarns (SSYs) as the active triboelectric layer. Owing to the built-in auxetic and core-shell conjugate structure design, contact and separation between the triboelectric materials become more effective, which contributes to more effective biomechanical energy harvesting from various deformation. To further enhance the output performance, barium titanate ($BaTiO_3$) nanoparticles and graphene were mixed into PDMS to largely improve the dielectric property for generating more charges. The prepared AXF-TENG was flexible, stretchable, stable and sensitive to versatile external mechanical stimuli such as stretching, compressing, and bending. To demonstrate its superior performance, a single AXF-TENG was used as a self- powered multifunctional sensor to detect joint-bending motions and integrated in a self- powered gesture- recognizing glove to detect finger motion states. Furthermore, AXF-TENGs were woven into an energy-

harvesting fabric to evaluate their capability of scavenging various types of energy from human motion for light up light emitting diodes (LEDs), charging commercial capacitors, powering electronic watch and scientific calculator. This work indicates the proposed AXF-TENGs hold promising potentials for versatile applications in biomechanical energy harvesting and self-powered human motion sensing.

2. Experimental Section

2.1 Materials

The silicone elastomer base and related curing agent for Polydimethylsiloxane (PDMS, SYLGARD® 184) were bought from Dow Chemical Company (USA). Stainless steel yarns (SSYs, Bekinox AISI 316L) were purchased from Bekaert (Belgium). Barium Titanate nanoparticles ($BaTiO_3$, cubic crystalline phase, < 100 nm particle size) was supplied by Aladdin (China). n-Hexane (95%, HPLC) was purchased from Sigma-Aldrich (USA), and graphene powder (diameter: 0.5 ~ 5 μm; thickness: ~ 0.8 nm; purity: ~ 99%) was purchased from Nanjing XFNANO Materials Tech Co., Ltd (China). Transparent PVC tube (inner diameter of 2 mm) was obtained from Shenzhen Woer Heat-shrinkable Material Co., LTD (China). Stainless steel tubular braided sleeves (diameter of 2 mm) were bought from Dongguan Changsheng Electric Technology Co., Ltd (China). All the materials were used as received without further purification.

2.2 Fabrication of the AXF-TENG

The fabrication processes for the coaxial core-shell AXF-TENG are illustrated in Figure 1. Firstly, silicone elastomer base and curing agent was mixed homogeneously by mechanical stirring for 30 min with a weight ratio of 10: 1 to prepare the PDMS mixture solution. Then, the mixture solution was placed in a vacuum oven at room temperature for 20 min to remove the bubbles. Afterward, stainless steel yarns (SSYs) were inserted into 10 cm PVC tubes with different pre-stretched strains (10%, 20%, 30% 40% and 50%) respectively (Figure 1a). Subsequently, both ends of each tube were capped with PDMS (Figure 1b) and pre-strains were released to construct inner helical-structured SSYs with different pitches (Figure 1c). Hereafter, PDMS mixture solution was drawn into a 10 mL plastic syringe and injected into the helical-structured SSYs-filled tubes (Figure 1d). After curing at 70 °C for 30 min in an oven, the PVC tubes were carefully peeled off by scissors (Figure 1e) to obtain PDMS-SSY fibers (Figure 1f). Following this, the prepared PDMS-SSY fibers were inserted into commercially hollow stainless steel braided sleeves (Figure 1g) and the two ends of these sleeves were encapsulated by the adhesive tapes (Figure 1h). According to the above operation procedures, AXF-TENGs with a core-shell coaxially structure was prepared.

To enhance the output performance, AXF-TENGs with BT-PDMS, Graphene-BT-PDMS composites were also prepared. Firstly, BT nanoparticles and graphene were dispersed in PDMS elastomer base at different BT mass ratios (10, 20, 30, 40, 50, 60, 70 wt.%) and different graphene mass ratios (0.05, 0.1, 0.2, 0.3, 0.4, 0.5, 0.6, 0.7, 0.8 wt.%), respectively. Secondly, the BT/PDMS composite mixture with 20 mL n-Hexane was magnetically stirred until the n-Hexane solvent totally volatilized. Afterward,

curing agent was added followed by stirring for another 30 min. Other procedures and conditions remain the same.

2.3 Characterization and Measurements

Photographs were taken with a digital camera (Nikon D5600). A scanning electron microscope (TESCAN VEGA3) operating at 20 kV was employed to investigate the morphology of AXF-TENG. An optical microscope (Olympus BX41) was used to observe the lateral expanding behavior of the auxetic PDMS-SSY fibers before and after stretching. To assess the auxetic behavior of different PDMS-SSY fibers, tensile measurements were performed on a universal tensile testing machine (Instron 4411) equipped with a 5 kN load cell. Photographs of the tested samples at different stretching strains during the tensile measurements were in-situ taken to measure the transversal deformations of samples. The output performance of AXF-TENG under impacting/releasing cycles was evaluated by utilizing a Keyboard Life Tester (ZX-A03). The output voltage signal was collected by Keysight DSO-X3014A oscilloscope and N2790A high voltage probe with 8 MΩ internal resistance. Open-circuit voltage and short-circuit current were measured using an electrometer (Keithley 6514).

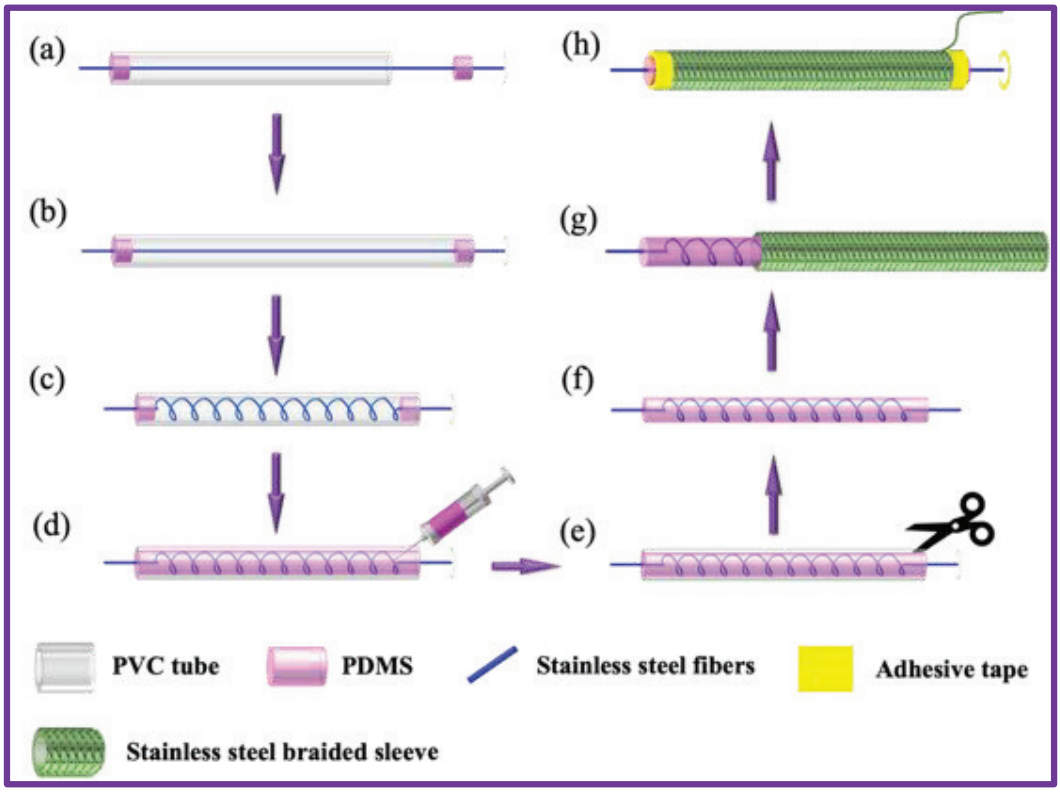

Figure 1. Schematic illustration of the fabrication process of coaxial core-shell AXF-TENG.

3. Results and Discussion

3.1 Preparation of the AXF-TENG

Figure 1 illustrates the detailed fabrication processes of the proposed AXF-TENG. Firstly, to fabricate the auxetic PDMS-SSY core fiber, SSY was inserted into a pre-stretched hollow PVC tube (Figure 1a). Then, both ends of each tube were capped with PDMS (Figure 1b) and pre-strains were released to construct helical-structured SSYs as inner electrode (Figure 1c). Subsequently, PDMS was injected into the SSY-filled PVC tube and cured in the oven to prepare PDMS-SSY core fiber (Figure 1d). After peeling off the PVC tube wall (Figure 1e), the prepared PDMS-SSY core fiber (Figure 1f) were inserted into a commercially hollow SSBS shell (Figure 1g) and encapsulated with adhesive tape at both ends to obtain the AXF-TENG (Figure 1h).

3.2 Working mechanism of the AXF-TENG

The schematic diagrams showing the vertical-section of the fabricated AXF-TENG before and after stretching are shown in Figure 2a and b. The AXF-TENG consists of an auxetic PDMS-SSY with negative Poisson's ratio as core fiber and a commercial SSBS with positive Poisson's ratio as outside shell. As shown in Figure 2b, the auxetic PDMS-SSY fiber would laterally expand when stretched. This special deformation behavior can be explained as follows: The prepared PDMS-SSY structure can be understood as a straight PDMS elastomeric core fiber with a stiffer SSY wound around it in a helical form[44]. Under the tensile force, the stiff SSY is straightened and displaces the core PDMS fiber into a crimped form, resulting in an expansion of the PDMS-SSY structure in the lateral direction[45].

The working mechanism of the fabricated AXF-TENG during stretching/releasing process is based on two electrodes contact-separate mode of the triboelectric effect, which are shown in Figure 2c-f. When a tensile force is applied on the AXF-TENG, the PDMS-SSY core fiber laterally expanded and effectively contacted with the laterally contracted SSBS shell electrode, causing triboelectrification. Since PDMS and SSBS shell are opposite on the triboelectric series, the PDMS would generate negative charges, while the SSBS shell would generate positive charges (Figure 2c). After the AXF-TENG was released from the stretched state, the PDMS-SSY core fiber would separate from the SSBS shell, returning to its original position. The charge separation would cause the PDMS to induce positive charges onto the SSY. This would drive electrons to flow from the SSBS shell electrode to the SSY through the external circuit

to reach electrostatic equilibrium, producing a positive current (Figure 2d). When the AXF-TENG was released to the original state, an equilibrium state was reached, and no free electrons would flow to produce current (Figure 2e). When the AXF-TENG was stretched again and the core-shell layers got close to each other, electrons would flow back from SSBS shell electrode to the SSY inner electrode (Figure 2f). This process generated a negative current until reaching a new equilibrium state with the core-shell layers in contact again (Figure 2c). In this way, an alternate current was generated during the repeated contact and separation process between PDMS-SSY core fiber and SSBS shell under a periodic tensile force.

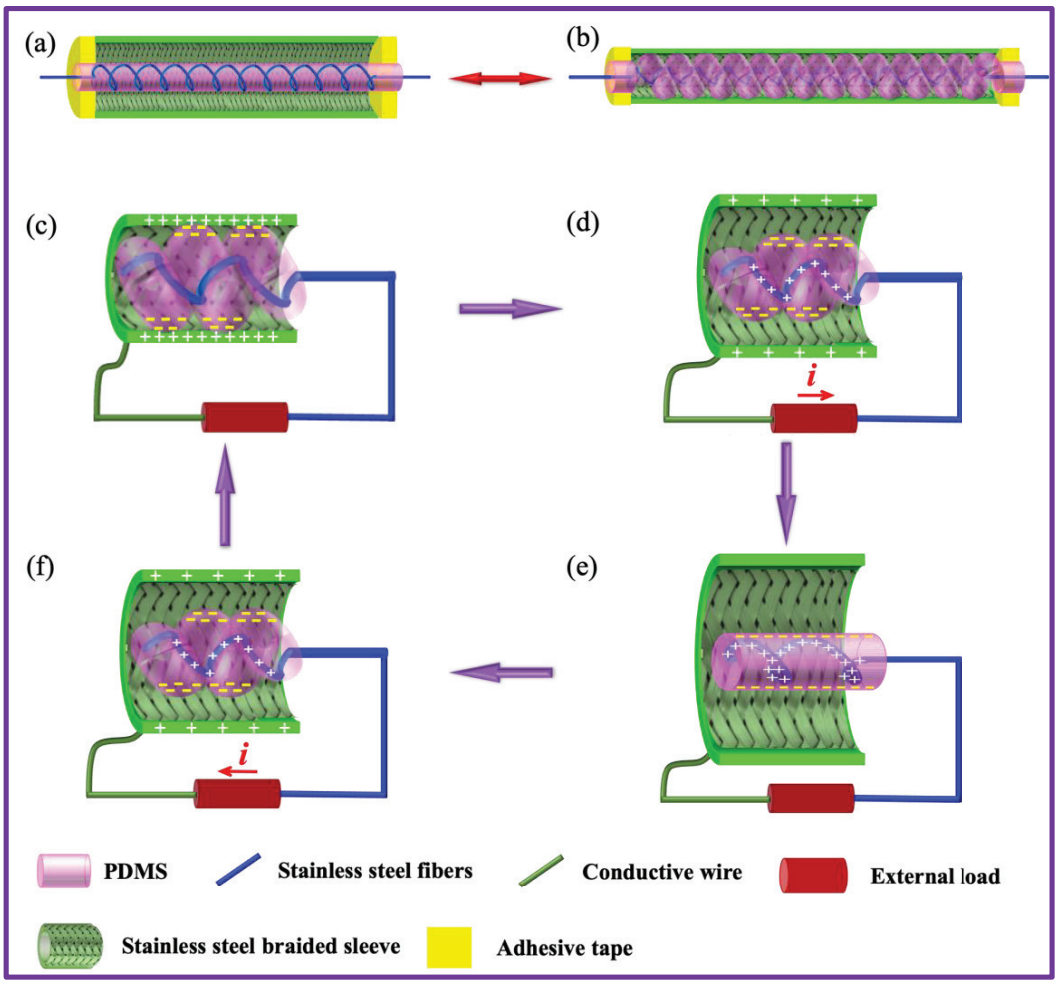

Figure 2. Schematic structure and working mechanism of AXF-TENG. (a-b) Schematic diagrams showing the structure of AXF-TENG before (a) and after (b) tensile deformation. (c-f) Schematic diagrams showing the working mechanism of triboelectric output of AXF-TENG during stretching/releasing process.

3.3 Characterization of the PDMS-SSY core fiber and SSBS shell

Figure 3a and Figure 3b show the cross-section morphology of PDMS-SSY core fiber at different magnifications. It can be seen that the helix structured SSY occurs at the inner edge of core PDMS matrix, which is then encapsulated by a thin layer of PDMS at the outmost side. Figure 3c shows the SEM image of the used SSY which not only serves as the inner electrode but also plays an important role in resulting negative Poisson's ratio effect.

The characteristics and properties of core fiber, such as number of coils (NOC), electrical conductivity, stretchability and Poisson's ratio under stretching, which have significant influence on the final performance of AXF-TENG, were carefully investigated. Figure 3d and Figure 3e show the optical images of the PDMS-SSY core fiber at unstretched state and stretched at a 15% strain, respectively. From the images, it is obvious that the core fiber expands in the latitudinal direction when it is stretched in the longitudinal direction. This is can be attributed to the rationally designed helical auxetic fiber (HAY) structure, which was formed with a straight elastomeric PDMS core, a stiffer SSY wound around it in a helical form, and a thin coating of PDMS (Figure 2a). Under stretching, the stiff SSY is straightened and displaces the PDMS

core into a crimped form, which results in an expansion of the fiber structure in the lateral direction (Figure 2b). The outmost PDMS sheath not only serves as good binder between PDMS core and SSY but also avoids short circuit from contact between SSY and SSBS shell under stretching.

Coil number of SSY plays a key role in the auxetic property of PDMS-SSY fiber. Therefore, a series of PDMS-SSY with different coil numbers were designed by pre-stretching the PVC tube to different levels of strains. As shown in Figure 3f, when pre-strain increases from 10% to 50%, coil number of SSY rises from 1.4 to 2.5/cm correspondingly. In addition, the electrical conductivity of inner SSY electrode during stretching, which is also crucial for AXF-TENG to obtain high performance undergoing a tensile strain, was investigated in detail. As shown in Figure 3g, the resistance of SSY electrodes with different coil numbers were measured as a function of tensile strain. It can be seen that the resistance of all SSY electrodes declines slightly when the strain is increased, which can be attributed to the enhanced electrical conductivity induced by the closer contact between stainless steel fibers within the yarn at higher stretching states. Moreover, the maximum value of tensile strain is proportional to coil number of SSY in the core fiber when coil number increases from 1.4 to 2.5/cm, which rises from 7% to 40%.

Since the use of the stiff SSY is the key reason that triggers auxetic effect in the PDMS-SSY fiber, it is noteworthy to investigate the influence of SSY coil number on the auxetic effect. As shown in Figure 3h and Figure 3i, the transverse strain-tensile

strain curves and Poisson's ratio-tensile strain curves for PDMS-SSY fibers with different coil numbers were measured for comparison. The transverse strain (ε_t) was calculated from Equation (1):

$$\varepsilon_t = \frac{H-H_0}{H_0} \quad (1)$$

where H and H_0 are effective transverse widths of the sample at the stretched and initial states, respectively. Afterwards, the Poisson's ratio (v) was calculated from Equation (2):

$$\nu = -\frac{\varepsilon_t}{\varepsilon_l} \quad (2)$$

where ε_t and ε_l are transverse strain and tensile strain of the sample, respectively. It can be seen that coil number has a significant influence on the auxetic effect of the PDMS-SSY structure. As shown in Figure 3h, transverse strains of all PDMS-SSY fiber with different coil numbers from 1.4 to 2.5/cm rise under a tensile loading, while the slope declines gradually as the coil number increases. By comparing the Poisson's ratio-strain curves of PDMS-SSY fibers with different coil numbers as shown in Figure 3i, it can be found that negative Poisson's ratio of all PDMS-SSY fibers firstly increases, reaches its maximum effect at a tensile strain of about 5%, and then decreases gradually as the strain further increases. Meanwhile, the maximum negative Poisson's ratio value of PDMS-SSY fibers declines significantly from -10 to -0.2 when the coil number increases from 1.4 to 2.5/cm. This can be understood as follows: The deformation mechanism of the PDMS-SSY structure from a straight form to a wave form is mainly

caused by the straightening of the helix SSY, and it is normal that increased coil number can cause the difficult activation of shape change in PDMS-SSY structure, thereby resulting a declined negative Poisson's ratio effect.

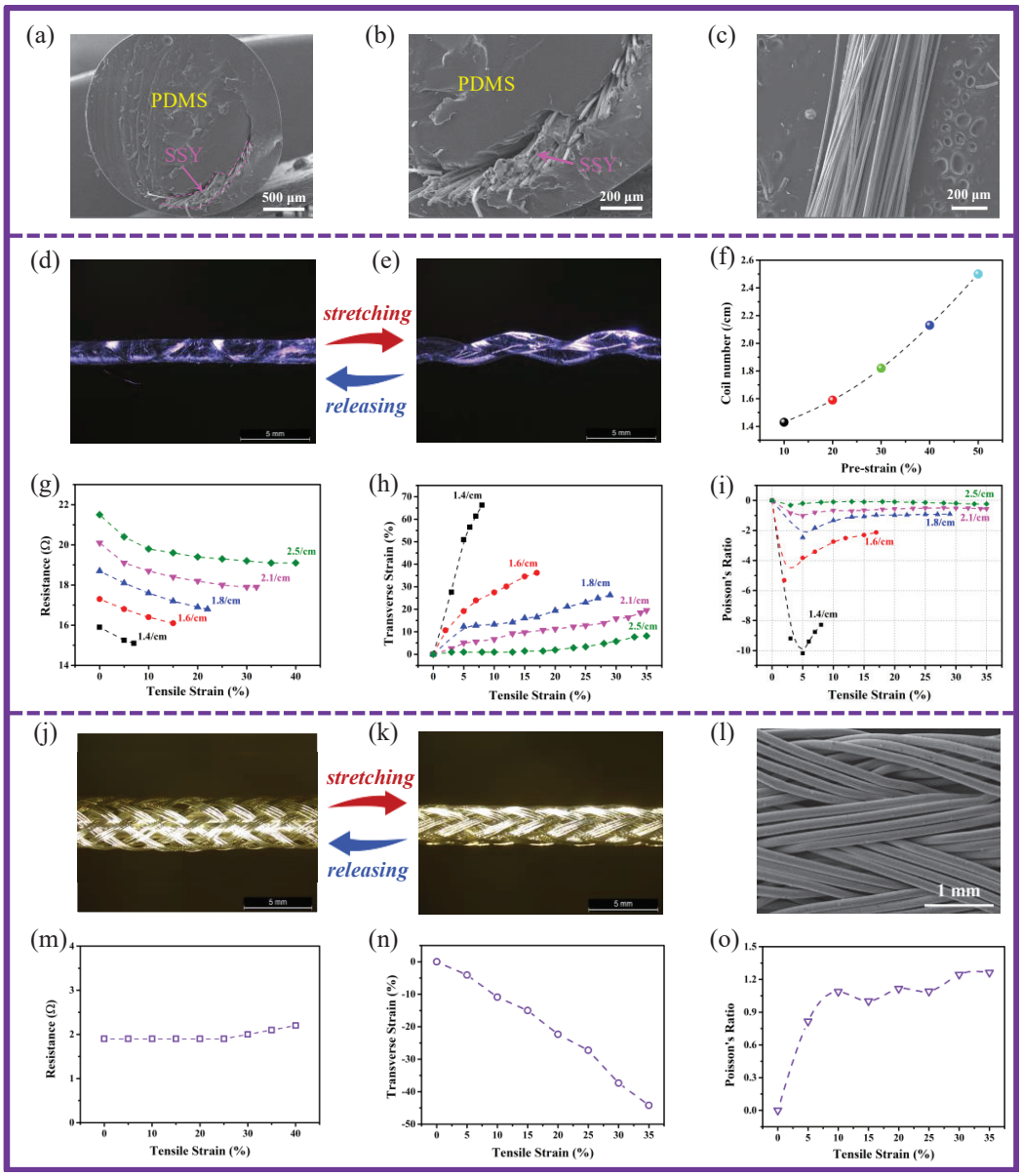

Figure 3 (a, b) The SEM images for the cross-sectional view of PDMS-SSY fiber at different magnifications. (c) The SEM image for the surface view of SSY. (d, e) Optical microscope photos of the core fiber (d) at the released state and (e) at the stretched state with 15% strain. (f) Coil

number dependence of the core fibers under different pre-strains. (g) Resistance, (h) transverse strain and (i) Poisson's ratio of the core fibers with different coil numbers under different tensile strains. (j-k) Optical microscope photos of the SSBS shell (j) at the released state and (k) at the stretched state with 35% strain. (l) SEM image of the surface morphology of the SSBS shell. (m) Resistance, (n) transverse strain and (o) Poisson's ratio of the SSBS shell under different tensile strains.

For comparison, the characteristics and properties of the SSBS shell under stretching were also investigated. As shown in Figure 3j and Figure 3k, it is obvious that the SSBS shell contracts in the latitudinal direction when it is stretched in the longitudinal direction, which behaves like a conventional braid. Figure 3l shows the surface morphology of the SSBS shell. Owing to the excellent electrical conductivity of stainless stain fibers, the resistance of SSBS shell shows no obvious changes during stretching (Figure 3m). In addition, the transverse strain and Poisson's ratio of SSBS shell were also been measured. The results show that the transverse width of SSBS shell shrinks to 50% of the initial value when the tensile strain increases to 35% (Figure 3n). Correspondingly, the Poisson's ratio of SSBS shell exhibits a positive Poisson's ratio under a tensile loading (Figure 3o). Therefore, by integrating it with the built-in auxetic PDMS-SSY core fiber into a core-shell conjugate structure design, contact and separation between the triboelectric materials would become more effective.

3.4 Output performance characterization

The output performance of the AXF-TENG was evaluated under a cyclic stretching

and releasing process. In order to obtain excellent outputs, the structure should be optimized. Number of coils (NOC) as one of the main factors, which played the key role in the auxetic property of core fiber, were investigated firstly. As shown in Figure 4a and Figure 4b, the frequency and tensile strain was fixed at 2 Hz and 5%, respectively, to investigate the influence of NOC on the outputs of AXF-TENG (~ 10 cm length). Due to the decreased Poisson's ratio of core fiber with the increase of NOC, the contact between core fiber and shell sleeve becomes more ineffective. Therefore, peak-to-peak open circuit voltage (V_{PP}) and short-circuit transfer charge (Q_{SC}) are both inversely proportional to NOC in the core fiber of AXF-TENG when NOC increases from 1.4 to 2.5/cm, which declines from ~ 6.7 V to ~ 1.6 V and from 1.9 nC to 0.6 nC, respectively. In order to investigate the output performance under different stretching strains, the NOC and stretch-release frequency were fixed at 1.8/cm and 2 Hz, respectively. As shown in Figure 4c and Figure 4d, with the increase of tensile strain from 5% to 25%, both the V_{PP} and Q_{SC} rise proportionally from ~ 3.8 to 24 V and from 1.2 to 6.5 nC, respectively. This can be attributed to the closer contact and enhanced triboelectric charges under higher tensile strain range. Furthermore, to systematically investigate the influence of stretch-release frequencies on electrical outputs, the AXF-TENG was measured at a fixed tensile strain of 25% and NOC of 1.8/cm. As shown in Figure 4e and Figure 4f, with the increase of stretch-release frequency from 0.5 to 5 Hz, both the V_{PP} and Q_{SC} do not experience obvious changes and stay at about 25 V and 6.5 nC, respectively, corresponding to the volumetric charge density of about 5.2 mC/m^3 and energy density of about 6.7 × 10^{-2} J/m^3 per cycle, respectively. This is because that V_{PP}

and Q_{SC} are mainly determined by the device structure and selected functional materials of TENGs. Therefore, when higher stretch-release frequency is applied, the whole transferred charges in each stretch-release cycle remains unchanged, producing a relatively constant V_{PP} and Q_{SC} outputs.

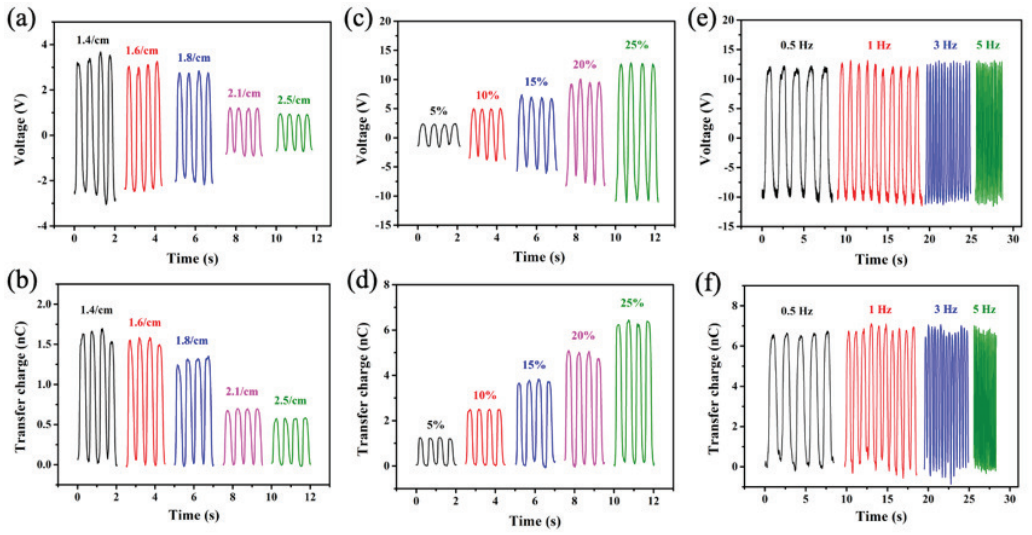

Figure 4 (a) Open-circuit voltage and (b) short-circuit transfer charge of the AXF-TENG with different number of coils, at 5% strain and 2 Hz frequency. (c) Open-circuit voltage and (d) short-circuit transfer charge of the AXF-TENG under various strain between 5% and 25%. (e) Open-circuit voltage and (f) short-circuit transfer charge of the AXF-TENG under various stretching frequency between 0.5 Hz and 5 Hz.

To further improve the electrical performance of the AXF-TENGs, PDMS based composites with higher relative permittivity were also applied to fabricate AXF-TENGs. For example, by adding different contents of $BaTiO_3$ nanoparticles (BT NPs) into PDMS matrix and dispersing homogeneously, $BaTiO_3$-PDMS composite (BT-PDMS) were prepared for preparing (BT-PDMS)-SSY core fibers. Figure 5a and Figure 5b show the optical images of the (BT-PDMS)-SSY core fiber (with BT content of 50 wt.% and NOC of 1.8/cm) at unstretched state and stretched at a 20% strain,

respectively. From the images, it is obvious that the (BT-PDMS)-SSY core fiber also expands in the latitudinal direction when it is stretched in the longitudinal direction. Figure 5c and Figure 5d show the cross-section morphology of (BT-PDMS)-SSY core fiber at different magnifications. It can be seen that BT NPs were well dispersed in PDMS matrix without obvious aggregation (Figure 5d). The elemental mapping of (BT-PDMS)-SSY in Figure 5e-e4 reveals the distribution of Ba, Ti, Si, and Fe elements. Here, the distributions of Ba and Ti are very uniform, which could be attributed to the well dispersion of $BaTiO_3$ in PDMS matrix. Figure 5f shows a typical BT-PDMS based AXF-TENG with the diameter of ~ 3.0 mm. In order to evaluate the flexibility of the BT-PDMS based AXF-TENG, flexibility measurements were conducted. As shown in Figure 5g-k, the BT-PDMS based AXF-TENG was capable of enduring various deformation states such as stretching (Figure 5g), bending (Figure 5h), twisting (Figure 5i), enwinding (Figure 5j) and knotting (Figure 5k), demonstrating its good flexibility and promising usability in wearable applications.

As the relative permittivity of the composites has significant influence on the electrical output performance of the AXF-TENG devices[46,47], the dielectric properties of the composites with BT NPs before and after the addition of graphene were investigated at the frequency of 320 kHz at room temperature. As shown in Figure 5l, the relative permittivity of BT-PDMS composites increased at first and then decreased with increasing BT NP content from 10 wt.% to 60 wt.%. The maximum relative permittivity arrived at 5.26 at the BT NP content of 50 wt.%. Afterwards, Graphene-BT-PDMS composites were prepared by adding different contents of

graphene into the BT (50 wt.%)-PDMS composite. Figure S1(a-c) show the cross-section morphology of Graphene (0.6 wt.%)-BT (50 wt.%)-PDMS-SSY core fiber at different magnifications and Figure S1(d-d5) show the elemental mapping of (BT-PDMS)-SSY. As shown in Figure 5m, with an increase in the graphene content, the relative constant of the samples firstly increased to a maximum of 9.87 (at graphene content of 0.6 wt.%) and then decreased. Figure 5n and Figure 5o show open-circuit voltage and short-circuit transfer charge of the AXF-TENG using PDMS, BT (50 wt.%)-PDMS, and Graphene (0.6 wt.%)-BT (50 wt.%)-PDMS under same NOC of 1.8/cm and stretching strain of 25% at 2 Hz. The results show that the electrical performance of AXF-TENGs can be significantly improved after adding BT NPs and graphene. Specifically, the peak-to-peak voltage and short-circuit transfer charge of BT (50 wt.%)-PDMS based AXF-TENG were ~ 36 V and ~ 11 nC, which were much higher than the values (~ 25 V, 6.5 nC). After adding graphene to further improve the relative permittivity of Graphene (0.6 wt.%)-BT (50 wt.%)-PDMS, the electrical performance could reach ~ 42 V and 12.5 nC, respectively. Furthermore, compared with other stretchable fiber-shaped TENGs in the previous published works (shown in Table S1 in the Supporting Information), the developed AXF-TENGs also exhibit superior electrical outputs. To demonstrate its flexibility and potential to harvest biomechanical energy and monitor human motions, a Graphene (0.6 wt.%)-BT (50 wt.%)-PDMS based AXF-TENG was fixed at various positions of human body to harvest energy from human motions. For example, at the elbow joint (Figure 5p), lateral elbow (Figure 5q) and knee joint (Figure 5r). The corresponding peak-to-peak voltage

can reach about 6 V (Figure 5p), 9 V (Figure 5q), and 17 V (Figure 5r), respectively. The long-term stability of TENG was also an important factor in practical application. As shown in Figure S2 in the Supporting Information, the output voltage of the BT-PDMS based AXF-TENG after 5,000 and 10,000 continuous stretching/releasing cycles can keep stable without obvious deterioration, showing that the prepared AXF-TENG has excellent stability and durability.

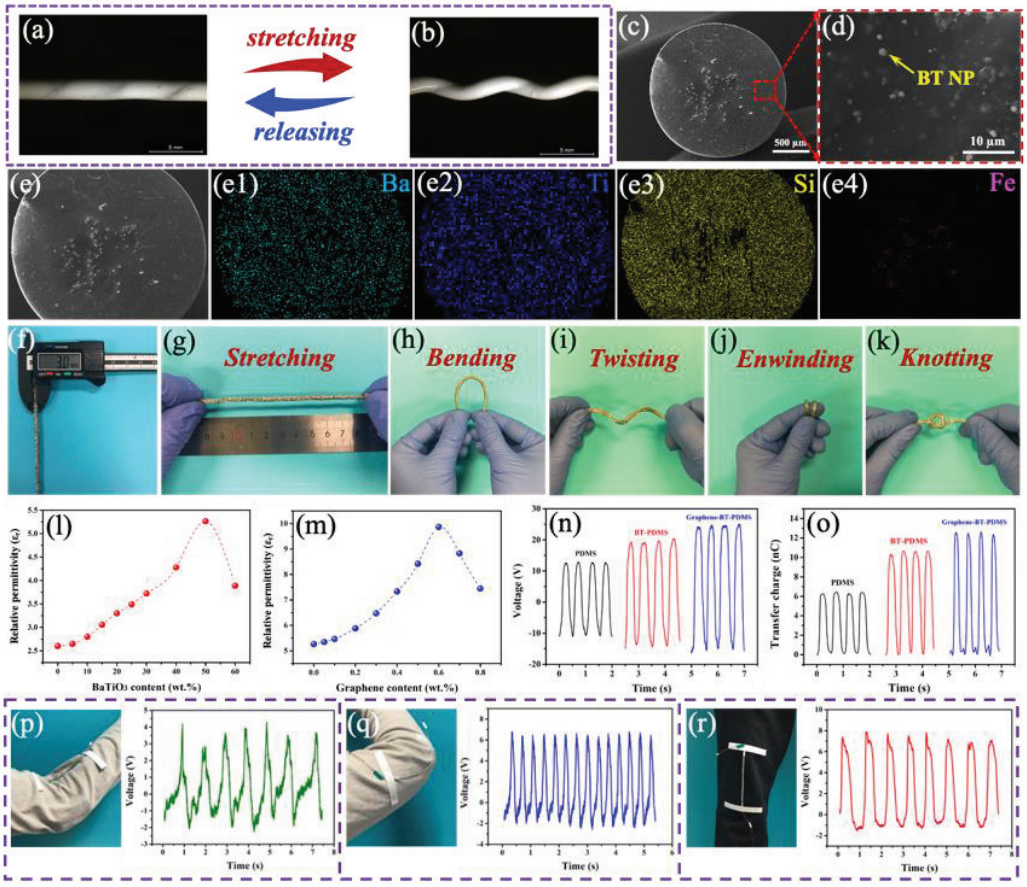

Figure 5 (a, b) Optical microscope photos of the BT-PDMS-SSY core fiber (a) at the released state and (b) at the stretched state with 20% strain. (c, d) The SEM images for the cross-sectional view of BT-PDMS-SSY fiber at different magnifications. (e-e4) Energy-dispersive X-ray spectroscopy mapping of different Ba, Ti, Si, and Fe elements in BT-PDMS-SSY. Photograph of the diameter measurement of AXF-TENG. Photographs of the AXF-TENG at (g) stretching, (h) bending, (i) twisting, (j) enwinding, and knotting states. (l) Relative permittivity variation of BT-PDMS composites versus $BaTiO_3$ NP weight ratio between 0% and 60%. (m) Relative permittivity

variation of Graphene-BT-PDMS composites (50 wt.% $BaTiO_3$ content) versus graphene weight ratio between 0% and 0.8%. (n) Open-circuit voltage and (o) short-circuit transfer charge of different AXF-TENGs with PDMS, BT (50 wt.%)-PDMS and Graphene (0.6 wt.%)-BT (50 wt.%)-PDMS as core triboelectric materials, at 25% strain and 2 Hz frequency. (c) Open-circuit voltage and (d) short-circuit transfer charge of the AXF-TENG under various strain (5-25%). (e) Open-circuit voltage and (f) short-circuit transfer charge of the AXF-TENG under various stretching frequency (0.5-5 Hz). Photographic images and open-circuit voltage of the Graphene (0.6 wt.%)-BT (50 wt.%)-PDMS based AXF-TENG fixed at different positions of human body: (p) at the elbow joint, (q) at the lateral elbow, and (r) at the knee joint.

3.5. Applications of the AXF-TENG

Furthermore, to demonstrate its application potential as a useful power source, a woven-structure AXF-TENG based textile was fabricated by weaving several BT-PDMS based AXF-TENGs and connecting all the electrodes of weft/warp yarns in parallel (Figure 6a). As shown in Figure 6b, the dependence of output performance of AXF-TENG based textile on external load resistances (R) under manually tapping has been systematically studied. It can be seen that output voltage (V) tends to increase with increasing load resistances, while the instantaneous power density increased at first and then decreased with increasing load resistances from 1 KΩ to 100 MΩ. The maximum instantaneous power density arrived at 52.36 mW/m^2 at a load resistance of about 10 MΩ. Through lightly tapping the AXF-TENG based textile by hand, the electric energy can directly drive 20 LEDs connected serially (Figure 6c and Movie S1). In addition, the rectified output signals of AXF-TENG based textile could be charged into several capacitors with different capacitances. Fig. 5d shows the voltage-charging curves of capacitors measured by tapping the AXF-TENG based textile. The voltages of 2 μF, 4.7 μF, and 22 μF capacitors can reach 3.0 V within 46 s, 83 s and 233 s,

respectively. With a simple bridge rectifier circuit (Figure 6e), the charged capacitor (22 μF) can easily power a digital watch (Figure 6f and Movie S2) and a calculator (Figure 6g and Movie S3), respectively. Above results clearly reveal the AXF-TENGs can effectively generate electrical output under various human motions and show promising potential for powering wearable electronics. Finally, a smart textile glove was made by stitching several BT-PDMS based AXF-TENGs onto the back of a commercial knitted cotton glove corresponding to the position of five fingers. To demonstrate its potential to detect finger movements, the AXF-TENGs on different finger positions were serial connected and output voltage signals under different circumstances were investigated. When any finger was bent and released periodically, the periodic contact area between BT-PDMS core fiber and stainless-steel sleeve increased and decreased at the same time. Thus, the real-time electrical output could indicate the different gestures, as shown in Figure 6h. It is obvious that the peak-to-peak voltage outputs of this smart glove increased when the number of bent fingers increased from one (~ 2.8 V) to two (~ 4.4 V), three (~ 7.5 V), four (~ 8.0 V), and five (~ 11.3 V), clearly affirming the feasibility of AXF-TENG based textile sensors in detection of human motions and recognition of different gestures.

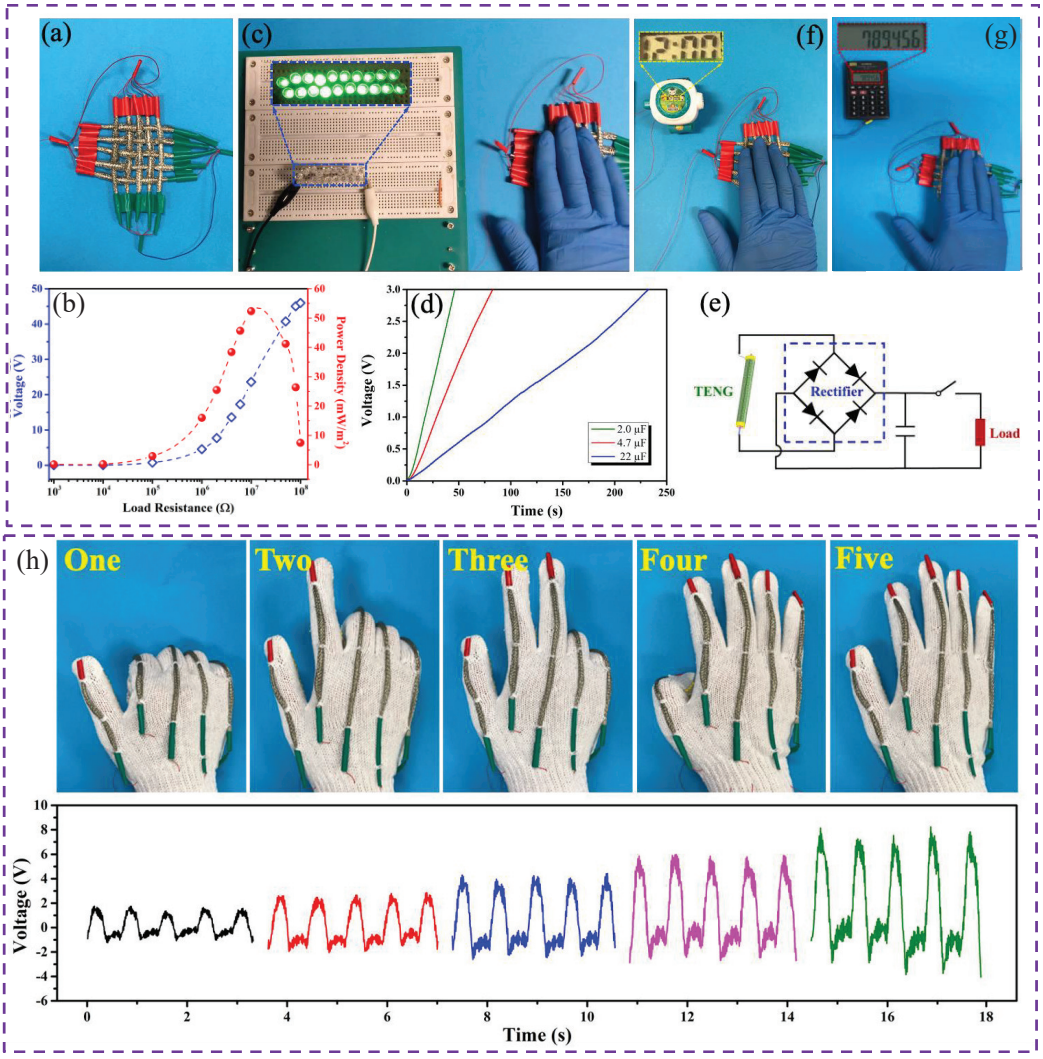

Figure 6 (a) Photograph of the AXF-TENG based fabric with 5 × 5 weaving patterns. (b) Dependence of the output voltage and instantaneous power density of the AXF-TENG based fabric on load resistances. (c-g) Demonstrations of the AXF-TENG based fabric as power source: (c) Photograph of directly lighting up 20 LEDs by the AXF-TENG based fabric under hand tapping; (d) Charging curves of 2, 4.7, and 22 μF capacitors by manually tapping the AXF-TENG based fabric; (e) The equivalent electrical circuit of the self-powered system; (f, g) Photographs of the self-powered system driving an electronic watch and a calculator, respectively. (h) Demonstration of the AXF-TENGs stitched in a smart glove for active gesture sensing application: voltage signals representing the numbers of "one", "two", "three", "four" and "five" by different gestures.

4. Conclusions

In summary, we have designed and developed a novel type of stretchable fiber-shaped

triboelectric nanogenerator with a core-shell coaxial architecture, in which a brand-new negative Poisson-ratio auxetic core fiber was axially inserted into a commercial hollow circular sleeve with positive Poisson's ratio, forming a unique synergistic structured TENG of opposite Poisson's ratios. Herein, the developed auxetic core fiber, which would expand in all directions under stretching, was rationally designed by selecting a helical-structure stainless steel yarn as the stretchable electrode and employing polydimethylsiloxane (PDMS) to cover the spiral stainless-steel yarns (SSYs) as the active triboelectric layer. Resultantly, contact and separation between the triboelectric materials become more effective, which contribute to harvesting more biomechanical energy from deformation. The prepared AXF-TENG was flexible, stretchable, stable and sensitive to versatile external mechanical stimuli such as stretching. Specifically, the output voltage and transferred charge of AXF-TENG can reach up to ~ 25 V and ~ 6.5 nC, respectively. By adding $BaTiO_3$ nanoparticles and graphene into PDMS matrix, the fabricated composites with largely improved the dielectric property could significantly improve the output voltage and transferred charge of AXF-TENGs to ~ 42 V and ~ 12.5 nC, respectively. Demonstration of applications showed that the proposed AXF-TENGs hold promising potentials for versatile applications in energy harvesting from human motions and are expected to be further employed in self-powered devices.

Acknowledgements

The authors would like to acknowledge the funding support from the Hong Kong

Polytechnic University (IWEAR and G-YWA2) for the work reported here.

References

[1] Y. Lee, J. Park, A. Choe, S. Cho, J. Kim, H. Ko, Mimicking Human and Biological Skins for Multifunctional Skin Electronics, Adv. Funct. Mater. 30 (2020) 1–32. https://doi.org/10.1002/adfm.201904523.

[2] Z. Lou, L. Wang, K. Jiang, Z. Wei, G. Shen, Reviews of wearable healthcare systems: Materials, devices and system integration, Mater. Sci. Eng. R Reports. 140 (2020). https://doi.org/10.1016/j.mser.2019.100523.

[3] H. Wu, Y.A. Huang, F. Xu, Y. Duan, Z. Yin, Energy Harvesters for Wearable and Stretchable Electronics: From Flexibility to Stretchability, Adv. Mater. 28 (2016) 9881–9919. https://doi.org/10.1002/adma.201602251.

[4] S.S. Kwak, H.J. Yoon, S.W. Kim, Textile-Based Triboelectric Nanogenerators for Self-Powered Wearable Electronics, Adv. Funct. Mater. 29 (2019) 1–26. https://doi.org/10.1002/adfm.201804533.

[5] Y. Chen, B. Xu, J. Gong, J. Wen, T. Hua, C.W. Kan, J. Deng, Design of High-Performance Wearable Energy and Sensor Electronics from Fiber Materials, ACS Appl. Mater. Interfaces. 11 (2019) 2120–2129. https://doi.org/10.1021/acsami.8b16167.

[6] J. Wen, B. Xu, J. Zhou, Y. Chen, Novel high-performance asymmetric supercapacitors based on nickel-cobalt composite and PPy for flexible and wearable energy storage, J. Power Sources. 402 (2018) 91–98.

https://doi.org/10.1016/j.jpowsour.2018.09.030.

[7] X. Guan, B. Xu, J. Gong, Hierarchically architected polydopamine modified BaTiO3@P(VDF-TrFE) nanocomposite fiber mats for flexible piezoelectric nanogenerators and self-powered sensors, Nano Energy. 70 (2020). https://doi.org/10.1016/j.nanoen.2020.104516.

[8] J. Gong, B. Xu, X. Guan, Y. Chen, S. Li, J. Feng, Towards truly wearable energy harvesters with full structural integrity of fiber materials, Nano Energy. 58 (2019) 365–374. https://doi.org/10.1016/j.nanoen.2019.01.056.

[9] X. Guan, B. Xu, M. Wu, T. Jing, Y. Yang, Y. Gao, Breathable, washable and wearable woven-structured triboelectric nanogenerators utilizing electrospun nanofibers for biomechanical energy harvesting and self-powered sensing, Nano Energy. 80 (2021). https://doi.org/10.1016/j.nanoen.2020.105549.

[10] W. Song, X. Fan, B. Xu, F. Yan, H. Cui, Q. Wei, R. Peng, L. Hong, J. Huang, Z. Ge, All-Solution-Processed Metal-Oxide-Free Flexible Organic Solar Cells with Over 10% Efficiency, Adv. Mater. 30 (2018) 1–8. https://doi.org/10.1002/adma.201800075.

[11] L. Zhang, S. Lin, T. Hua, B. Huang, S. Liu, X. Tao, Fiber-Based Thermoelectric Generators: Materials, Device Structures, Fabrication, Characterization, and Applications, Adv. Energy Mater. 8 (2018) 1–18. https://doi.org/10.1002/aenm.201700524.

[12] T. He, X. Guo, C. Lee, Flourishing energy harvesters for future body sensor

network: from single to multiple energy sources, IScience. 24 (2021) 101934. https://doi.org/10.1016/j.isci.2020.101934.

[13] F.R. Fan, Z.Q. Tian, Z. Lin Wang, Flexible triboelectric generator, Nano Energy. 1 (2012) 328–334. https://doi.org/10.1016/j.nanoen.2012.01.004.

[14] F.R. Fan, L. Lin, G. Zhu, W. Wu, R. Zhang, Z.L. Wang, Transparent triboelectric nanogenerators and self-powered pressure sensors based on micropatterned plastic films, Nano Lett. 12 (2012) 3109–3114. https://doi.org/10.1021/nl300988z.

[15] J. Xiong, P. Cui, X. Chen, J. Wang, K. Parida, M.F. Lin, P.S. Lee, Skin-touch-actuated textile-based triboelectric nanogenerator with black phosphorus for durable biomechanical energy harvesting, Nat. Commun. 9 (2018) 1–9. https://doi.org/10.1038/s41467-018-06759-0.

[16] X. Guan, J. Gong, B. Xu, Three-Dimensional Conformal Porous Microstructural Engineering of Textile Substrates with Customized Functions of Brick Materials and Inherent Advantages of Textiles, ACS Appl. Mater. Interfaces. 12 (2020) 17967–17978. https://doi.org/10.1021/acsami.0c01557.

[17] Z. Lou, L. Li, L. Wang, G. Shen, Recent Progress of Self-Powered Sensing Systems for Wearable Electronics, Small. 13 (2017) 1–27. https://doi.org/10.1002/smll.201701791.

[18] T. He, Q. Shi, H. Wang, F. Wen, T. Chen, J. Ouyang, C. Lee, Beyond energy harvesting - multi-functional triboelectric nanosensors on a textile, Nano Energy.

57 (2019) 338–352. https://doi.org/10.1016/j.nanoen.2018.12.032.

[19] J. Zhu, M. Zhu, Q. Shi, F. Wen, L. Liu, B. Dong, A. Haroun, Y. Yang, P. Vachon, X. Guo, T. He, C. Lee, Progress in TENG technology—A journey from energy harvesting to nanoenergy and nanosystem, EcoMat. 2 (2020) 1–45. https://doi.org/10.1002/eom2.12058.

[20] L. Jin, B. Zhang, L. Zhang, W. Yang, Nanogenerator as new energy technology for self-powered intelligent transportation system, Nano Energy. 66 (2019). https://doi.org/10.1016/j.nanoen.2019.104086.

[21] M. Zhu, T. He, C. Lee, Technologies toward next generation human machine interfaces: From machine learning enhanced tactile sensing to neuromorphic sensory systems, Appl. Phys. Rev. 7 (2020) 031305. https://doi.org/10.1063/5.0016485.

[22] Y. Cheng, X. Lu, K. Hoe Chan, R. Wang, Z. Cao, J. Sun, G. Wei Ho, A stretchable fiber nanogenerator for versatile mechanical energy harvesting and self-powered full-range personal healthcare monitoring, Nano Energy. 41 (2017) 511–518. https://doi.org/10.1016/j.nanoen.2017.10.010.

[23] W. Gong, C. Hou, J. Zhou, Y. Guo, W. Zhang, Y. Li, Q. Zhang, H. Wang, Continuous and scalable manufacture of amphibious energy yarns and textiles, Nat. Commun. 10 (2019) 1–8. https://doi.org/10.1038/s41467-019-08846-2.

[24] C. Wu, T.W. Kim, F. Li, T. Guo, Wearable Electricity Generators Fabricated Utilizing Transparent Electronic Textiles Based on Polyester/Ag

Nanowires/Graphene Core-Shell Nanocomposites, ACS Nano. 10 (2016) 6449–6457. https://doi.org/10.1021/acsnano.5b08137.

[25] W.B. Ko, D.S. Choi, C.H. Lee, J.Y. Yang, G.S. Yoon, J.P. Hong, Hierarchically Nanostructured 1D Conductive Bundle Yarn-Based Triboelectric Nanogenerators, Adv. Mater. 29 (2017) 1–9. https://doi.org/10.1002/adma.201704434.

[26] J. Wang, S. Li, F. Yi, Y. Zi, J. Lin, X. Wang, Y. Xu, Z.L. Wang, Sustainably powering wearable electronics solely by biomechanical energy, Nat. Commun. 7 (2016) 1–8. https://doi.org/10.1038/ncomms12744.

[27] K. Dong, Z. Wu, J. Deng, A.C. Wang, H. Zou, C. Chen, D. Hu, B. Gu, B. Sun, Z.L. Wang, A Stretchable Yarn Embedded Triboelectric Nanogenerator as Electronic Skin for Biomechanical Energy Harvesting and Multifunctional Pressure Sensing, Adv. Mater. 30 (2018) 1–12. https://doi.org/10.1002/adma.201804944.

[28] J. Park, A.Y. Choi, C.J. Lee, D. Kim, Y.T. Kim, Highly stretchable fiber-based single-electrode triboelectric nanogenerator for wearable devices, RSC Adv. 7 (2017) 54829–54834. https://doi.org/10.1039/c7ra10285b.

[29] X. Li, Z.H. Lin, G. Cheng, X. Wen, Y. Liu, S. Niu, Z.L. Wang, 3D fiber-based hybrid nanogenerator for energy harvesting and as a self-powered pressure sensor, ACS Nano. 8 (2014) 10674–10681. https://doi.org/10.1021/nn504243j.

[30] J. Zhong, Y. Zhang, Q. Zhong, Q. Hu, B. Hu, Z.L. Wang, J. Zhou, Fiber-based

generator for wearable electronics and mobile medication, ACS Nano. 8 (2014) 6273–6280. https://doi.org/10.1021/nn501732z.

[31] H.J. Sim, C. Choi, S.H. Kim, K.M. Kim, C.J. Lee, Y.T. Kim, X. Lepró, R.H. Baughman, S.J. Kim, Stretchable Triboelectric Fiber for Self-powered Kinematic Sensing Textile, Sci. Rep. 6 (2016) 1–7. https://doi.org/10.1038/srep35153.

[32] A. Yu, X. Pu, R. Wen, M. Liu, T. Zhou, K. Zhang, Y. Zhang, J. Zhai, W. Hu, Z.L. Wang, Core-Shell-Yarn-Based Triboelectric Nanogenerator Textiles as Power Cloths, ACS Nano. 11 (2017) 12764–12771. https://doi.org/10.1021/acsnano.7b07534.

[33] K. Dong, Y.C. Wang, J. Deng, Y. Dai, S.L. Zhang, H. Zou, B. Gu, B. Sun, Z.L. Wang, A Highly Stretchable and Washable All-Yarn-Based Self-Charging Knitting Power Textile Composed of Fiber Triboelectric Nanogenerators and Supercapacitors, ACS Nano. 11 (2017) 9490–9499. https://doi.org/10.1021/acsnano.7b05317.

[34] X. Fan, N. Wang, J. Wang, B. Xu, F. Yan, Highly sensitive, durable and stretchable plastic strain sensors using sandwich structures of PEDOT:PSS and an elastomer, Mater. Chem. Front. 2 (2018) 355–361. https://doi.org/10.1039/c7qm00497d.

[35] J. Li, B. Xu, Novel highly sensitive and wearable pressure sensors from conductive three-dimensional fabric structures, Smart Mater. Struct. 24 (2015)

125022. https://doi.org/10.1088/0964-1726/24/12/125022.

[36] J. Zhong, Q. Zhong, Q. Hu, N. Wu, W. Li, B. Wang, B. Hu, J. Zhou, Stretchable Self-Powered Fiber-Based Strain Sensor, Adv. Funct. Mater. 25 (2015) 1798–1803. https://doi.org/10.1002/adfm.201404087.

[37] Y. Yang, L. Xie, Z. Wen, C. Chen, X. Chen, A. Wei, P. Cheng, X. Xie, X. Sun, Coaxial Triboelectric Nanogenerator and Supercapacitor Fiber-Based Self-Charging Power Fabric, ACS Appl. Mater. Interfaces. 10 (2018) 42356–42362. https://doi.org/10.1021/acsami.8b15104.

[38] L. Xie, X. Chen, Z. Wen, Y. Yang, J. Shi, C. Chen, M. Peng, Y. Liu, X. Sun, Spiral Steel Wire Based Fiber-Shaped Stretchable and Tailorable Triboelectric Nanogenerator for Wearable Power Source and Active Gesture Sensor, Nano-Micro Lett. 11 (2019) 3–12. https://doi.org/10.1007/s40820-019-0271-3.

[39] K. Dong, J. Deng, W. Ding, A.C. Wang, P. Wang, C. Cheng, Y.C. Wang, L. Jin, B. Gu, B. Sun, Z.L. Wang, Versatile Core–Sheath Yarn for Sustainable Biomechanical Energy Harvesting and Real-Time Human-Interactive Sensing, Adv. Energy Mater. 8 (2018) 1–12. https://doi.org/10.1002/aenm.201801114.

[40] D. Kim, J. Park, Y.T. Kim, Core-Shell and Helical-Structured Cylindrical Triboelectric Nanogenerator for Wearable Energy Harvesting, ACS Appl. Energy Mater. 2 (2019) 1357–1362. https://doi.org/10.1021/acsaem.8b01931.

[41] X. Yu, J. Pan, J. Zhang, H. Sun, S. He, L. Qiu, H. Lou, X. Sun, H. Peng, A coaxial triboelectric nanogenerator fiber for energy harvesting and sensing under

deformation, J. Mater. Chem. A. 5 (2017) 6032–6037. https://doi.org/10.1039/c7ta00248c.

[42] X. He, Y. Zi, H. Guo, H. Zheng, Y. Xi, C. Wu, J. Wang, W. Zhang, C. Lu, Z.L. Wang, A Highly Stretchable Fiber-Based Triboelectric Nanogenerator for Self-Powered Wearable Electronics, Adv. Funct. Mater. 27 (2017) 1–8. https://doi.org/10.1002/adfm.201604378.

[43] S.L. Zhang, Y.C. Lai, X. He, R. Liu, Y. Zi, Z.L. Wang, Auxetic Foam-Based Contact-Mode Triboelectric Nanogenerator with Highly Sensitive Self-Powered Strain Sensing Capabilities to Monitor Human Body Movement, Adv. Funct. Mater. 27 (2017) 1–7. https://doi.org/10.1002/adfm.201606695.

[44] N. Jiang, H. Hu, Auxetic Yarn Made with Circular Braiding Technology, Phys. Status Solidi. 256 (2019) 1800168. https://doi.org/10.1002/pssb.201800168.

[45] N. Jiang, H. Hu, A study of tubular braided structure with negative Poisson's ratio behavior, Text. Res. J. 88 (2018) 2810–2824. https://doi.org/10.1177/0040517517732086.

[46] T. Jing, B. Xu, Y. Yang, C. Jiang, M. Wu, Interfacial modification boosted permittivity and triboelectric performance of liquid doping composites for high-performance flexible triboelectric nanogenerators, Nano Energy. 78 (2020) 105374. https://doi.org/10.1016/j.nanoen.2020.105374.

[47] T. Jing, B. Xu, Y. Yang, Liquid doping materials as micro-carrier of functional molecules for functionalization of triboelectric materials and flexible

triboelectric nanogenerators for energy harvesting and gesture detection, Nano Energy. 74 (2020) 104856. https://doi.org/10.1016/j.nanoen.2020.104856.